Published in final edited form as:
J Mol Biol. 2008 February 1; 375(5): 1329–1343. doi:10.1016/j.jmb.2007.11.037.

AKAP18 contains a phosphoesterase domain which binds AMP

Matthew G. Gold[1], **F. Donelson Smith**[2], **John D. Scott**[2], and **David Barford**[1,3]

[1]Section of Structural Biology, Institute of Cancer Research, Chester Beatty Laboratories, 237 Fulham Road, London, SW3 6JB, UK

[2]Howard Hughes Medical Institute, Vollum Institute, Oregon Health and Science University, Portland OR-97239, USA

SUMMARY

Protein kinase A anchoring proteins (AKAPs), defined by their capacity to target the cAMP-dependent protein kinase to distinct sub-cellular locations, function as molecular scaffolds mediating the assembly of multi-component complexes to integrate and organise multiple signalling events. Despite their central importance in regulating cellular processes, little is known regarding their diverse structures and molecular mechanisms. Here, using bioinformatics and X-ray crystallography, we define a central domain of AKAP18δ (AKAP18^{CD}) as a member of the 2H phosphoesterase family. The domain features two conserved His-x-Thr motifs positioned at the base of a groove located between two lobes related by pseudo two-fold symmetry. Nucleotide co-crystallisation screening revealed that this groove binds specifically to 5'AMP/CMP, with the affinity constant for AMP in the physiological concentration range. This is the first example of an AKAP capable of binding a small molecule. Our data generate two functional hypotheses for the AKAP18 central domain. It may act as a phosphoesterase, although we did not identify a substrate, or as an AMP sensor with the potential to couple intracellular AMP levels to PKA signalling events.

Keywords

AKAP; PKA; scaffold; AMP; phosphoesterase

INTRODUCTION

Synthesis of the intracellular second messenger cAMP by adenylyl cyclase stimulates activation of cAMP-binding proteins such as cyclic nucleotide-gated channels[1] and Epac guanine nucleotide exchange factors[2], with the principal intracellular target being protein kinase A (PKA)[3]. Although cAMP is diffusible, rises in cAMP concentration are restricted to microdomains of the cell[4]. A-kinase Anchoring Proteins (AKAPs) organise signalling within cAMP microdomains by anchoring multiple signalling proteins[5], which in addition to PKA and other signalling proteins, include the enzymes responsible for cAMP synthesis[6]

[3]Corresponding author: David Barford, David.barford@icr.ac.uk, Tel: +44 (0)20 7153 5420, FAX: + 44 (0)20 7153 5457.

PDB accession codes: 2VFY (APO), 2VFK (5'AMP complex), 2VFL (5'CMP complex)

and breakdown[7]. Recent investigations of AKAPs challenge the view of scaffold proteins as inert platforms that merely co-localise discrete subsets of proteins.

Despite considerable structural and functional diversity, all AKAPs share three common properties: an amphipathic helix to anchor the PKA holoenzyme through interaction with the N-terminal Docking/Dimerisation (D/D) domain of its regulatory (R) subunits[8–10]; targeting elements to particular subcellular locations; and the ability to bind other signalling proteins[5]. Subcellular location of AKAPs is often dynamic, for example AKAP79 is released from the cell membrane following rises in calcium concentration and activation of calmodulin[11]. The ability of AKAPs to bind multiple proteins provides a mechanism to integrate different second messenger signals, for example AKAP-Lbc inputs signals from both protein kinase C and PKA to activate protein kinase D[12]. AKAPs may also modulate the properties of bound proteins, for example 3-phosphoinositide protein kinase 1 is activated upon engaging mAKAP[13] and Yotiao can directly increase the current passing through the heart potassium channel IK_5 (Ref [14]). Consistent with their role in organising signalling complexes, AKAPs are involved in important biological processes, for example AKAP79 targets PKA and protein phosphatase 2B for respective phosphorylation and dephosphorylation of a glutamate receptor critical in hippocampal synaptic plasticity[15,16], and mAKAP anchors an array of signalling enzymes[17] for regulation of various aspects of heart function including calcium release from the sarcoplasmic reticulum[18].

Many AKAPs are expressed as alternatively spliced isoforms. The AKAP15/18 gene encodes four splice variants (Supplementary Figure S1) that range in size from 15–37 kDa. These anchoring proteins utilise distinct targeting motifs to determine specific subcellular locations[19–21]. Membrane targeting of the α and β variants is mediated by lipid modification of sites at the extreme amino terminus[22,23] whereas the larger δ variant is predominantly cytoplasmic[24]. Under certain circumstances, the AKAP18γ variant is believed to reside in the nucleus[25]. Nonetheless, all four variants contain an R subunit-binding helix, which binds both PKA regulatory subunit isoforms[19–21], and a putative leucine zipper motif that anchors at least the α isoform to L-type calcium channels[26]. AKAP18α plays a role in the brain, where it directs PKA toward neuronal sodium channels[27] allowing their dopaminergic modulation[28]. More recently, the δ isoform has been shown to anchor PKA for both phosphorylation of aquaporin-2 at Ser-256 following vasopressin stimulation in the kidney[29], and phosphorylation of phospholamaban in the heart[30]. AKAP18δ has also been reported to bind to PDE4D isoforms through elements within its central region[31].

Knowledge of the three-dimensional structures of proteins provides crucial insights into protein function unavailable from other techniques. However, structural information for AKAPs has to date been limited to studies of the AKAP-PKA interaction[8–10]. For a variety of reasons AKAPs are challenging targets for crystallographic investigation. AKAPs are often large proteins that can be difficult to express in bacteria. Generally, AKAP sequences are thought to be of low complexity, containing few discrete globular folded domains. Additional problems arise because most AKAPs simultaneously interact with multiple binding partners, so heterologous expression in their absence may destabilise protein structure and increase protein degradation.

To define features in AKAPs that might be amenable to structural analysis, we analysed mammalian AKAPs by a bioinformatics approach to identify putative globular domains. Here, we present the identification and structure determination of a central domain (~200 residues) common to AKAP18γ/δ (termed $AKAP18^{CD}$). Our results, the first crystal structure of an AKAP domain, reveal a structural resemblance to the 2H phosphoesterase family, proteins that harbour a pair of conserved His-x-Thr motifs. Members of this family include RNA ligases and cyclic nucleotide phosphoesterases. Characterisation of the domain

revealed that AKAP18^{CD} specifically interacts with 5'AMP and CMP, but lacks a range of phosphoesterase activities. These data suggest that AKAP18δ acts either as a phosphoesterase for an unidentified substrate, or that the protein functions as an AMP sensor, thereby coupling intracellular AMP levels with PKA-mediated phosphorylation processes.

RESULTS

AKAP18δ incorporates a 2H phosphoesterase domain

The longest splice variant of each known mammalian AKAP (20 proteins) was analysed using the secondary structure prediction program JPRED[32] and the protein tertiary structure recognition program PHYRE[33] (Table 1). Regions of discrete non-repetitive secondary structure were predicted by JPRED, for example a C-terminal region in AKAP95 (approximately residues 360–692) and throughout the short AKAP, AKAP28. Protein fold recognition analysis indicated regions of potential architectural similarity to proteins of known structure. Domains detected in some AKAPs had previously been characterised (for example the RhoGEF domain of AKAP-Lbc), whereas in other AKAPs, novel domain definitions using PHYRE were strongly supported by high (>40%) sequence identity with the identified structural homolog (for example the Sec7 domain in BIG2). Structural analysis of these regions would be less likely to yield much in the way of new functional information. Of more interest was the detection of structural homology within AKAPs to proteins of known fold, not clearly evident from sequence analysis alone. These included the long AKAP18 isoforms γ and δ, identified as incorporating a central domain likely to resemble members of the 2H phosphoesterase family, despite the absence of significant sequence similarity (17%)(Table 1).

To address the structural and functional properties of AKAP18δ three constructs for bacterial expression of rat AKAP18δ were designed corresponding to full-length protein, an N-terminal truncation (residues 76–357) and the limited central domain (76–292), termed AKAP18^{CD} (Supplementary Figure S1). The central domain was purified by glutathione affinity and gel filtration chromatography, whereas the longer proteins eluted in the void volume on gel filtration, and were not investigated further. AKAP18^{CD} was crystallised by hanging drop vapour diffusion, and the structure was determined at 1.8 Å resolution by single isomorphous replacement with anomalous scattering (SIRAS). Data collection, phasing and refinement statistics are listed in Table 2.

AKAP18^{CD} adopts a globular α-β type architecture consisting of four α-helices and eight β-sheets, with approximate dimensions of 50 × 40 × 30 Å. The domain is bilobal with two four-stranded antiparallel β-sheets at its core related by a pseudo two-fold rotational symmetry (Figure 1A). A deep water-lined groove lies between the two lobes and penetrates approximately 15 Å into one face of the protein. The strands β2 and β5 run antiparallel to each other at the base of this groove (Figure 1A), and each harbours a His-x-Thr motif that defines the 2H phosphoesterase family[34] and is conserved in AKAP18γ/δ across species (Figure 1B).

The side-chains of residues Arg219 and Thr220 (arginine-containing 'R' loop, connecting α3 to β5, Figure 1A) are not visible in the electron density map and the main-chain atoms of these residues are relatively mobile ($<B>_{main\text{-}chain}$ of 40.4 Å^2 for residues 219 and 220 compared to overall $<B>_{main\text{-}chain}$ of 30.0 Å^2). This region lies at one entrance to the groove, adjacent to another flexible loop region (residues 179–182, connecting β3 and β4) that also possesses relatively high B-factors ($<B>_{main\text{-}chain}$ of 37.8 Å^2).

AKAP18δ binds 5'AMP and 5'CMP specifically

Because 2H phosphoesterases catalyse reactions involving nucleotides, we tested the nucleotide-binding capability of AKAP18δ by co-crystallising $AKAP18^{CD}$ in the presence of a variety of nucleotides. In each instance, a complete dataset was collected at higher than 2.5 Å resolution, and the presence of nucleotide was detected by determining the structure by molecular replacement. Significantly, electron density characteristic of nucleotide was visible in F_o-F_c difference maps when $AKAP18^{CD}$ was co-crystallised in the presence of either 5 mM adenosine 5'-monophosphate (5'AMP) or cytosine 5'-monophosphate (5'CMP). However, there was no electron density suggestive of nucleotide after co-crystallisation with a range of other nucleotides, including 3'AMP, guanosine 5'-monophosphate (5'GMP) and thymidine 5'-monophosphate (5'TMP), as listed in Figure 2A. Co-crystallisation with decreasing concentrations of 5'AMP indicated that the ligand binds with a dissociation constant (K_d) in the mid-micromolar range (Figure 2A).

The affinity constant for 5'AMP was more accurately quantified by equilibrium fluorescence binding using the AMP derivative 2'- (or 3'-)-*O*-(*N*-methylanthraniloyl) adenosine 5'-monophosphate (MANT-AMP). MANT fluoresces at 448 nm upon excitation near 335 nm, which allows protein binding to be detected by FRET upon excitation at 290 nm. A plot of the difference in fluorescence in the presence and absence of $AKAP18^{CD}$ over a range of MANT-AMP concentrations reveals the fraction of $AKAP18^{CD}$ that is bound to MANT-AMP at a given concentration. As the concentration of $AKAP18^{CD}$ (25 μM) is low, the K_d for MANT-AMP can be approximated by fitting the data to a hyperbolic function. Iterative rounds of least square fitting modelled the data shown in Figure 2B to the function:

$$\Delta F = 92.8\,[\mathrm{MANT-AMP}]/(194+[\mathrm{MANT-AMP}])$$

to give a K_d of 194 +/− 30 μM (n=3). This value agrees with the results of the 5'AMP co-crystallisation titrations, where electron density was visible for bound 5'AMP when at 670 μM but not at 40 μM. Immobilisation of different AKAP18δ fragments to 5'AMP-coupled agarose demonstrated that the central domain is necessary for binding 5'AMP (Figure 2C).

To understand the molecular basis for preferential binding to 5'AMP/CMP rather than 5'GMP/TMP, structures of $AKAP18^{CD}$ in complex with 5'AMP and 5'CMP were refined at 1.5 and 2.25 Å resolution, respectively. Data collection and refinement statistics for these complex crystal structures are listed in Table 2. In both complexes, nucleotide binds within the deep groove of the AKAP18δ central domain with the phosphate moiety coordinated by the two His-x-Thr motifs, and the base moiety contacted by residues from the β3/β4 and R-loops (Figure 3).

Coordination of the identical ribose and phosphate moieties of 5'AMP and 5'CMP by $AKAP18^{CD}$ is very similar. At the base of the groove, the two His-x-Thr motifs dominate interactions to the nucleotide phosphate group via a network of direct and water-mediated hydrogen bonds (Figure 4A). The two threonines (134 and 226) of the His-x-Thr motifs donate direct hydrogen bonds to phosphate oxygen atoms, whereas His224 of the second His-x-Thr motif donates a hydrogen bond to the ester oxygen. Water-mediated hydrogen bonds to phosphate oxygen atoms are provided by the side chain amine of Lys229 and by main chain amide (Thr134) and carbonyl (His132) groups. The only interaction to the ribose moiety is a van der Waals contact with Val183 (Figure 4A). This residue, like the majority of the residues lining the groove, is invariant in AKAP18 across all species (Figure 1B). The ribose hydroxyl groups of 5'AMP are solvent accessible (Figure 3B).

The base moieties of both 5'AMP and 5'CMP are sandwiched between the side-chains of Phe179 and Arg219, at one entrance to the groove (Figure 4B, C). Arg219 forms a cation–π interaction with the adenine moiety of 5'AMP (Figure 3B, 4B) and with the cytidine moiety of 5'CMP (Figure 4C), an interaction known to stabilise protein-DNA complexes, while Phe179 forms a π-stacking interaction on the opposite side of the base. The binding of nucleotide stabilises and immobilises the loops harbouring Phe179 (β3/β4 loop) and Arg219 (R loop), with concomitant ordering of the side-chains of Arg219 and Thr220. Two water-mediated protein-base hydrogen bonds are also visible in the 5'AMP complex structure: adenine position N6 to the main-chain carbonyl of Thr220 and position N7 to the main-chain amide of Lys222 (Figure 4B). Residues involved in the coordination of phosphate and adenosine moieties of 5'AMP/CMP are respectively labelled with black and red triangles in the sequence alignment (Figure 1B).

The coordination of 5'AMP and 5'CMP suggests that a contact between the backbone carbonyl of Thr220 and the group attached to C6 (purine, Figure 4B) or C4 (pyrimidine, Figure 4C) of the base provides base-specificity for AKAP18δ. In the 5'AMP complex, the amine in this position is 3.5 Å from the carbonyl of Thr220 (Figure 4B); the equivalent distance is 4.1 Å for the 5'CMP complex (Figure 4C). Both are close enough that substitution of carbonyl for amine, as in guanine and thymidine, would cause a repulsive interaction with the carbonyl of Thr220, accounting for the specificity of AKAP18δ for 5'AMP and 5'CMP.

We performed further co-crystallisations to explore nucleotide specificity. ATP, ADP and NADP did not associate with AKAP18^{CD}. These results may be rationalised from the coordination observed for the mononucleotides 5'AMP and 5'CMP; there is no space for the additional phosphate group of a dinucleotide. The cyclic nucleotides 3'–5' cAMP, its non-hydrolysable analogue Rp-cAMPS, and the cyclic nucleotides cyclic 2'–3' cytosine monophosphate (2'–3' cCMP) and cyclic 2'–3' nicotinamide diphosphate (2'–3' cNADP) also failed to bind when present at 5 mM in the crystallisation solution (Figure 2A). Any of these cyclic nucleotides would be unable to satisfy the precise network of hydrogen bonds coordinating the phosphate and ribose moieties in the 5'AMP complex (Figure 4A). The nucleotide-binding properties that we observed in the crystal are likely to be a true reflection of the binding capabilities of AKAP18δ as the highly conserved groove region is not influenced by crystal lattice contacts.

AKAP18^{CD} resembles bacterial 2'–5' RNA ligases

The DALI server (http://www.ebi.ac.uk/dali/)[35] was used to search for structural homologues of AKAP18^{CD} (Supplementary Table S1) (Figure 5). As expected, the domain aligned with 2H phosphoesterase proteins. The closest superpositions were to bacterial 2'–5' RNA ligases from *Pyrococcus horikoshii*[36] and *Thermus thermophilus*[37]. The domain also superposed well with *Arabidopsis thalania* 1'–2'-cyclic nucleotide 2'-phosphodiesterase[38], although less well to goldfish[39] and human[40] brain 2'–3'-cyclic nucleotide 3'-phosphodiesterases.

The existence of the 2H phosphoesterase protein superfamily has been recognised for some time[34], but the functions of the various superfamily members remain poorly understood. The 2'–5' RNA ligases, catalyse the ligation of half-tRNA molecules with 2'3'-cyclic phosphate and 5'-hydroxyl termini (Figure 6A). *A. thalania* 1'–2'-cyclic nucleotide 2'-phosphodiesterase hydrolyses ADP-ribose 1",2"-cyclic phosphate (Appr>r), a product of the tRNA splicing reaction (Hoffman *et al*., 2000) (Figure 6B). Brain 2'–3'-cyclic nucleotide 3'-phosphodiesterase remains an enigma – its physiological substrate is still unknown despite considerable investigation of its biological roles. Although the protein is capable of hydrolysing the cyclic phosphodiester of the unphysiological molecule cyclic 2'–3'NADP,

its role as a PDE is controversial. The 2H phosphoesterase superfamily comprises ten sub-families, with four major clades[41]. AKAP18δ is assigned to the eukaryotic LigT sub-family comprising eight members. One of these, the human protein activating co-integrator 1, which assembles into a four subunit transcription co-activator complex[42], bears little similarity to AKAP18δ except for the central His-x-Thr motifs. Interestingly, some superfamily members are coupled to UBA and SH3 domains suggesting a possible function in signal transduction.

Structural alignment of the AKAP18δ binding groove with homologous 2H phosphoesterases (Figure 5) indicates that numerous highly conserved residues are shared between AKAP18δ (Figure 5A) and 2'–5' ligases from *P. horikoshii* (Figure 5B)[36] and *T. thermophilus* (Figure 5C)[37]. Equivalent residues for both His-x-Thr motifs, Phe179, Val183 and Tyr280 are positioned within the 2'–5' RNA ligase binding grooves (Figures. 5B, C). Lys229 in AKAP18δ is replaced by arginine in the RNA ligases, a conservative substitution, and Val137 is replaced by phenylalanine (Figures. 5B, C). Arg219 in the AKAP18δ R-loop is replaced by either glycine (Figure 5B) or lysine (Figure 5C) in the 2'–5' RNA ligases. Apart from the His-x-Thr motifs, AKAP18^{CD} is less similar to *A. thalania* 1'–2'-cyclic nucleotide 2'-phosphodiesterase[38,43]. Specifically there are no counterparts to Arg219 and Phe179 (Figure 5D). Finally, the AKAP18δ binding groove bears little similarity to 2'–3'-cyclic nucleotide 3'-phosphodiesterases[39,40].

AKAP18δ lacks a range of cyclic nucleotide phosphoesterase activities

All known 2H phosphoesterase catalytic reactions involve nucleophilic attack of a cyclic phosphate, although the product of the reaction varies depending on the attacking group and linkage positions of the substrate phosphodiester. A putative mechanism for the *T. thermophilus* 2'–5' RNA ligase has been proposed[37] (Figure 6A). His130 functions to activate the 5' hydroxyl of a tRNA half-molecule for nucleophilic attack onto the cyclic phosphate of a second tRNA half-molecule. Thr41, Thr132 and Arg135 are proposed to anchor the cyclic phosphate, while His39 protonates the 2"-oxygen of the cyclic phosphate and promotes P-O bond cleavage. In this instance, the product of the reaction is the linkage of two RNA half-molecules via a 2'–5' phosphodiester bond[37]. Since residues lining the AKAP18δ groove (Figure 5A) are conserved with 2'–5' RNA ligase (Figure 5C), the AKAP18δ – 5'AMP complex crystal structure, serves as a model to elaborate the proposed catalytic model[37]. It is likely that Phe80 and Val88 of the ligase (equivalent to Phe179 and Val183 of AKAP18δ), respectively coordinate the base and ribose moieties of the 3' tRNA half-molecule (Figure 6A). Furthermore, Arg135 (Lys229 of AKAP18δ) is suitably positioned to allow for stabilisation of a pentaphosphate transition state (Figure 6A). This geometry suggests that Phe44 (Figure 5C), on the other side of the binding groove, is likely to be involved in coordinating the 5' tRNA half-molecule.

In AKAP18δ, the presence of both His-x-Thr motifs could enable activation of a water or 5'-hydroxyl group for nucleophilic attack, and protonation of a leaving oxygen group to complete the catalytic reaction. Interestingly His132, the putative acid (Figure 6A), is conserved and not involved in contacts to 5'AMP (Figure 4A). Potentially important distinctions between the AKAP18δ and 2'–5' RNA ligase binding grooves are the positions of phenylalanine and lysine/glycine (Figures 5C, 6A) in the ligases at the equivalent positions to Val137 and Arg219, respectively of AKAP18δ (Figures 5A, 6C). Residues of AKAP18δ remote from the binding groove share less than 15% identity with the 2'–5' RNA ligases. The catalytic mechanism of *A. thalania* 1'–2'-cyclic nucleotide 2'-phosphodiesterase[38,43] is similar although in this instance water is activated for nucleophilic attack and the cyclic phosphate forms ester bonds at 1'–2' (Figure 6B). The crystal structure of *A. thalania* CNP in complex with cyclic 2'–3' uridine vanadate (cU-V)[43] (Figure 5D) reveals that, in a similar manner to the AKAP18-AMP complex (Figure 5A), the His-x-Thr

motifs are responsible for coordinating the oxyanion moiety of the nucleotide, although in this instance the phosphate is replaced by vanadate and is cyclised between the 2'–3' ribose positions. The base and ribose moieties of cU-V are coordinated differently, in comparison to 5'AMP in complex with AKAP18, which enables the cyclic vanadate to be accommodated (Supplementary Figure S2). In both complexes, phenylalanine residues, although located differently (Phe84 in the *A. thalania* CNP, Figure 5D; Phe179 in AKAP18, Figure 5A), are important for coordinating the base moiety.

In an attempt to test the possibility that AKAP18δ can function as a 2'–5' RNA ligase, crystallisation of $AKAP18^{CD}$ was performed in the presence of two nucleotides which, according to the reaction mechanism illustrated in Figure 6A, would be expected to bind to $AKAP18^{CD}$ when present at high concentration. Co-crystallisations were performed with 5 mM 3'AMP, to mimic the tRNA 3' half-molecule (Figure 6D), and with 5 mM 2'–3' cCMP, to mimic the tRNA 5' half-molecule (Figure 6E). Neither nucleotide bound to $AKAP18^{CD}$ (Figure 2A). These results are inconsistent with the notion that AKAP18δ functions as a 2'5' RNA ligase. Furthermore, there is no existing evidence that AKAP18δ binds RNA or is involved in any form of RNA processing.

Given the ability of AKAP18δ to bind 5'AMP, a product of 3'5' cAMP hydrolysis, the capacity of 2H phosphoesterases to hydrolyse phosphodiesters with different ribose linkages, and the role of AKAP18 in anchoring PKA that responds to 3'–5' cAMP, we tested the hypothesis that the AKAP18δ central domain might function as a 3'–5' cAMP phosphodiesterase. However, AKAP18δ displayed no cAMP or cGMP phosphodiesterase activity regardless of the cyclic nucleotide concentration or pH tested (Figure 6F), a finding consistent with the lack of binding of 3'5' cAMP in the crystal (Figure 2A).

DISCUSSION

In this study we have, to our knowledge, performed the first systematic bioinformatics analysis to define domain structures within the AKAP superfamily. Using protein fold recognition approaches, we identified domains within AKAPs that had not been recognised previously. Some novel domain definitions are supported by a high degree of sequence similarity to structural homologs, whereas for others, the degree of sequence similarity is not statistically significant. We defined one such domain of AKAP18γ/δ as belonging to the 2H phosphoesterase family. Crystallographic analysis of $AKAP18^{CD}$ confirmed this prediction, providing the first structural information concerning a functional domain within an AKAP. Nucleotide binding experiments indicate that $AKAP18^{CD}$ specifically interacts with 5'AMP and 5'CMP.

Our studies indicate two possible biological functions for the central domain of AKAP18δ. Its resemblance to tRNA ligases and CNPs of the 2H phosphoesterase family suggests that it either hydrolyses or ligates cyclic nucleotide phosphodiesters, however we could not detect catalytic activity associated with the protein. The other possibility is that AKAP18δ acts as a 5'AMP effector. 5'AMP functions as an energy sensor to mediate cell signalling, with increased AMP concentrations triggering the activation of both AMP kinase[44] and glycogen phosphorylase[45]. 5'AMP stimulates AMP kinase with an EC_{50} in the low micromolar range[46], whereas glycogen phosphorylase is converted to the activated conformation with an EC_{50} of ~75 μM in the absence of glucose 6-phosphate[47]. In contrast, the affinity of $AKAP18^{CD}$ for AMP is slightly lower. Its affinity for 5'AMP is likely to be similar to that of MANT-AMP (K_d of 194 μM), as the 2' and 3' ribose hydroxyl groups, modified in MANT-AMP, are accessible, unhindered by protein contacts (Figure 3B).

If we assume that the central domain of AKAP18δ acts as a 5'AMP sensor, how might 5'AMP propagate an effect on binding to the protein? Structural rearrangements on engaging 5'AMP are restricted to ordering of the R-loop and a small shift in position of the loop harbouring Lys229 (Figure 7A). Binding of 5'AMP also alters the shape and charge of the protein surface. Both hydroxyl groups of the 5'AMP ribose moiety are available for interaction, and nucleotide binding neutralises a region of positive charge at the base of the binding groove. A region comprising highly conserved residues (CR2) including residues Asp266-Gln275, lies adjacent to the binding groove (Figures 1A, 7B), and could potentially be involved in AKAP18δ-mediated inter-molecular interactions.

5'AMP binding might affect AKAP18δ activity in multiple ways. The conformational change and altered surface properties accompanying AMP binding could modulate the protein's cellular localisation. One possibility is an influence on the nuclear localisation of the protein, reminiscent of ligand-mediated nuclear targeting of steroid hormone receptors[48]. AKAP18γ/δ comprise a conserved nuclear localisation sequence (NLS)[49] immediately N-terminal to the central domain (Figure 1B)[25]. Mutation of the NLS prevents nuclear localisation of AKAP18γ expressed in HEK293 cells[25]. The NLS sequence, although present in AKAP18^{CD}, was not visible in the electron density. The most N-terminal residue with discernible electron density is Tyr88 whose Cα-atom is positioned 12 Å from the ribose 2'-hydroxyl group in the AKAP18δ – 5'AMP complex structure (Figure 7A), consistent with the possibility that the NLS could interact with elements involved in forming the AKAP18δ – 5'AMP complex. There are other targeting mechanisms that could be subject to 5'AMP regulation: AKAP18δ is present on aquaporin 2-bearing vesicles in the kidney[29], although the basis of this targeting is unknown. Alternatively, 5'AMP could affect the interaction of AKAP18δ with an associated protein. Recently, the AKAP18δ central domain was shown to interact with PDE4D3/9[31], however we could not detect an influence of 1 mM AMP on AKAP18δ interactions with either PDE4D6 or the PKA regulatory RII subunits (data not shown).

The phosphoesterase domain presented here is the first structure of a domain within an AKAP, and is the first demonstration of an AKAP with the ability to bind a small molecule. The 5'AMP complex structure provides insight into the mechanism of 2'–5' RNA ligases and should prove useful in understanding other members of the 2H phosphoesterase superfamily. These studies generate two functional hypotheses for AKAP18δ. First, the protein may act enzymatically as a phosphoesterase, although we did not identify a substrate. Alternatively, AKAP18δ may play a role as an AMP sensor, thereby coupling a metabolite effector protein with the primary intracellular receptor for cAMP (PKA). Our findings demonstrate the use of a combined bioinformatic-structural approach for uncovering new properties in proteins, and reveal another layer to the sophistication of AKAPs.

MATERIALS AND METHODS

Protein expression and purification

Three constructs of rat AKAP18δ (IMAGE I.D. 7315112) spanning the full-length protein (1–353), central domain (76–292, AKAP18^{CD}) and an N-terminal truncate (76–353) were cloned into pGEX6P1 and expressed as PreScission™-cleavable GST-fusion protein (GE healthcare) from *E. coli* BL21 Codon Plus® (DE3) cells (Stratagene). Cells were induced at OD_{600nm} = 0.5 with 0.5 mM IPTG and harvested after 16 hours at 18°C. Cells were lysed by sonication and following centrifugation the supernatant fraction was applied to 5 ml Glutathione Sepharose™ beads (GE healthcare). Bound recombinant protein was cleaved from the beads overnight with PreScission™ protease (GE healthcare), and applied to a Superdex 75 gel filtration column (GE healthcare) in 15 mM Tris-HCl (pH 7.5), 150 mM

NaCl, 0.1 mM EDTA and 2 mM DTT. The central domain eluted as a single peak on gel filtration. Selenomethionine-substituted AKAP18^{CD} was produced in B834 (DE3) and purified as the native protein. Mouse PDE4D6 (90–518) (IMAGE I.D. 23274169) was produced by the same protocol. His-tagged AKAP18δ (76–353) was expressed in *Sf*9 insect cells using the Bac-to-Bac Baculovirus Expression System (Invitrogen).

Crystallography

The best diffracting crystals grew in 0.1 M Tris HCl pH 8, 10 % PEG 8K, 7 mM DTT by hanging drop vapour diffusion at 14°C. Crystals were harvested after one week. For cryoprotection, crystals were immersed for 2 min in 0.1 M Tris HCl pH 8, 10% PEG 8K, 7 mM DTT, 75 mM NaCl and 25% glycerol, and then flash frozen at 100 K. Native and selenomethionine-substituted data were collected at ESRF.

Crystallographic programs were accessed via the CCP4 suite[50] - data was processed using MOSFLM and scaled and merged in SCALA (see Table 2 for details). Phases and initial electron density maps were calculated by SIRAS using SHELX and automatic model-building was performed using ArpWarp before final rounds of manual model-building and refinement using COOT[51] and REFMAC. Nucleotide co-crystallisation experiments were performed by including the specified concentration of nucleotide in both the precipitant solution and cryobuffer. Crystals were harvested after one week, and structures were solved by PHASER molecular replacement with, and REFMAC refinement against, the apo structure. The presence of bound nucleotide was determined by inspection of the difference F_o-F_c electron density map in COOT. Complexes with 5'AMP and 5' CMP were further refined with REFMAC. Nucleotide and side-chains for residues 219–220, invisible in the apo structure, were visible in the difference F_o-F_c electron density maps, so modelled in COOT before final refinement using REFMAC. Molecular representations in figures were created using The PyMOL Molecular Graphics System (DeLano Scientific, http://www.pymol.org) and BioDraw 10.0 (Merck).

cAMP phosphodiesterase assays

V5 epitope-tagged constructs of AKAP18δ and PDE4D3 were transiently expressed in HEK293 cells. Immunoprecipitates were washed three times (20 mM Tris HCl, pH 7.4) before incubation at 30°C for 10 min with 10 μM ^{3}H-cAMP in 20 mM Tris HCl, pH 7.4, 10 mM $MgCl_2$. The reaction was stopped by boiling for two minutes and ^{3}H-5'AMP was further hydrolysed to ^{3}H-adenosine by incubation with snake venom nucleotidase (Sigma). Finally ^{3}H-cAMP was removed by anion exchange (Biorad AG 1-X2) before scintillation counting. To assay cAMP activity in GST pull-downs, the [^{3}H] cAMP SPA Enzyme Assay (GE healthcare) was performed, following the manufacturer's guidelines.

Equilibrium fluorescence measurements

A Cary Eclipse fluorescence spectrophotometer (Varian) was used to measure fluorescence at 448 nm after excitation at 290 nm with increasing concentrations of MANT-AMP (Biolog) in the presence and absence of purified AKAP18^{CD}. A plot of the difference in fluorescence (ΔF) in the presence and absence of AKAP18δ ($F_{MANT} - F_{MANT+AKAP18\delta}$) over a range of MANT-AMP concentrations reveals the fraction of AKAP18δ that is bound to MANT-AMP at a given concentration. As the concentration of AKAP18δ (25 μM) is low, the K_d for MANT-AMP binding can be approximated by fitting the data to a hyperbolic function according to the equation:

$$\Delta F = B_0[\mathrm{MANT-AMP}]/(K_d + [\mathrm{MANT-AMP}])$$

where B_0 is the maximum change in fluorescence. ΔF was plotted as a function of [MANT-AMP] and fit to a hyperbolic function by least-squares using Origin software in order to determine the K_d.

Pull-down assays

Pull-down assays were performed using GST-fusion proteins immobilised to glutathione sepharose fast flow beads (GE Healthcare), and with 5'AMP-agarose (Sigma). For GST fusion pull-downs, GST-fusion protein was immobilised to the beads and washed with [500 mM NaCl, 25 mM TrisHCl pH 7.5, 2 mM DTT, 0.5 mM EDTA]. Protein samples were then mixed with the beads in low salt buffer [150 mM NaCl, 25 mM TrisHCl pH 7.5, 2 mM DTT, 0.5 mM EDTA, 0.05 % Tween-20]. After washing away non-specifically bound protein in low salt buffer, bound protein was detected by western blotting, or cAMP phosphodiesterase assay in the case of PDE4D6. Pull-down with immobilised GST alone was routinely included as a negative control for pull-downs using GST fusion proteins.

Supplementary Material

Refer to Web version on PubMed Central for supplementary material.

Acknowledgments

The work has been funded by a Medical Research Council studentship (MGG), and grants from CR-UK to DB and the NIH (GM48231) to JDS. We thank Richard Bayliss for assistance in the use of the fluorescence spectrophotometer.

REFERENCES

1. Houslay MD, Adams DR. PDE4 cAMP phosphodiesterases: modular enzymes that orchestrate signalling cross-talk, desensitization and compartmentalization. Biochem. J. 2003; 370:1–18. [PubMed: 12444918]
2. Bos JL. Epac: a new cAMP target and new avenues in cAMP research. Nat. Rev. Mol. Cell Biol. 2003; 4:733–738. [PubMed: 14506476]
3. Beavo JA, Brunton LL. Cyclic nucleotide research -- still expanding after half a century. Nat Rev Mol Cell Biol. 2002; 3:710–718. [PubMed: 12209131]
4. Zaccolo M, Pozzan T. Discrete microdomains with high concentration of cAMP in stimulated rat neonatal cardiac myocytes. Science. 2002; 295:1711–1715. [PubMed: 11872839]
5. Wong W, Scott JD. AKAP signalling complexes: focal points in space and time. Nat Rev Mol Cell Biol. 2004; 5:959–970. [PubMed: 15573134]
6. Bauman AL, et al. Dynamic regulation of cAMP synthesis through anchored PKA-adenylyl cyclase V/VI complexes. Mol Cell. 2006; 23:925–931. [PubMed: 16973443]
7. Dodge KL, et al. mAKAP assembles a protein kinase A/PDE4 phosphodiesterase cAMP signaling module. Embo J. 2001; 20:1921–1930. [PubMed: 11296225]
8. Carr DW, et al. Interaction of the regulatory subunit (RII) of cAMP-dependent protein kinase with RII-anchoring proteins occurs through an amphipathic helix binding motif. J. Biol. Chem. 1991; 266:14188–14192. [PubMed: 1860836]
9. Gold MG, et al. Molecular basis of AKAP specificity for PKA regulatory subunits. Mol Cell. 2006; 24:383–395. [PubMed: 17081989]
10. Kinderman FS, et al. A dynamic mechanism for AKAP binding to RII isoforms of cAMP-dependent protein kinase. Mol Cell. 2006; 24:397–408. [PubMed: 17081990]
11. Dell'Acqua ML, Faux MC, Thorburn J, Thorburn A, Scott JD. Membrane-targeting sequences on AKAP79 bind phosphatidylinositol-4, 5-bisphosphate. Embo J. 1998; 17:2246–2260. [PubMed: 9545238]
12. Carnegie GK, Smith FD, McConnachie G, Langeberg LK, Scott JD. AKAP-Lbc Nucleates a Protein Kinase D Activation Scaffold. Mol Cell. 2004; 15:889–899. [PubMed: 15383279]

13. Michel JJ, et al. Spatial restriction of PDK1 activation cascades by anchoring to mAKAPalpha. Mol Cell. 2005; 20:661–672. [PubMed: 16337591]
14. Kurokawa J, Motoike HK, Rao J, Kass RS. Regulatory actions of the A-kinase anchoring protein Yotiao on a heart potassium channel downstream of PKA phosphorylation. Proc Natl Acad Sci U S A. 2004; 101:16374–16378. [PubMed: 15528278]
15. Klauck TM, et al. Coordination of three signaling enzymes by AKAP79, a mammalian scaffold protein. Science. 1996; 271:1589–1592. [PubMed: 8599116]
16. Colledge M, et al. Targeting of PKA to glutamate receptors through a MAGUK-AKAP complex. Neuron. 2000; 27:107–119. [PubMed: 10939335]
17. Dodge-Kafka KL, et al. The protein kinase A anchoring protein mAKAP coordinates two integrated cAMP effector pathways. Nature. 2005; 437:574–578. [PubMed: 16177794]
18. Marx SO, et al. PKA phosphorylation dissociates FKBP12.6 from the calcium release channel (ryanodine receptor): defective regulation in failing hearts. Cell. 2000; 101:365–376. [PubMed: 10830164]
19. Fraser ID, et al. A novel lipid-anchored A-kinase Anchoring Protein facilitates cAMP- responsive membrane events. Embo J. 1998; 17:2261–2272. [PubMed: 9545239]
20. Gray PC, Scott JD, Catterall WA. Regulation of ion channels by cAMP-dependent protein kinase and A-kinase anchoring proteins. Curr. Opin. Neurobiol. 1998; 8:330–334. [PubMed: 9687361]
21. Trotter KW, et al. Alternative splicing regulates the subcellular localization of A-kinase anchoring protein 18 isoforms. J. Cell Biol. 1999; 147:1481–1492. [PubMed: 10613906]
22. Fraser ID, et al. A novel lipid-anchored A-kinase Anchoring Protein facilitates cAMP-responsive membrane events. Embo J. 1998; 17:2261–2272. [PubMed: 9545239]
23. Gray PC, et al. Primary structure and function of an A kinase anchoring protein associated with calcium channels. Neuron. 1998; 20:1017–1026. [PubMed: 9620705]
24. Trotter KW, et al. Alternative splicing regulates the subcellular localization of A-kinase anchoring protein 18 isoforms. J Cell Biol. 1999; 147:1481–1492. [PubMed: 10613906]
25. Brown RL, August SL, Williams CJ, Moss SB. AKAP7gamma is a nuclear RI-binding AKAP. Biochem Biophys Res Commun. 2003; 306:394–401. [PubMed: 12804576]
26. Hulme JT, Ahn M, Hauschka SD, Scheuer T, Catterall WA. A novel leucine zipper targets AKAP15 and cyclic AMP-dependent protein kinase to the C terminus of the skeletal muscle Ca2+ channel and modulates its function. J Biol Chem. 2002; 277:4079–4087. [PubMed: 11733497]
27. Tibbs VC, Gray PC, Catterall WA, Murphy BJ. AKAP15 anchors cAMP-dependent protein kinase to brain sodium channels. J Biol Chem. 1998; 273:25783–25788. [PubMed: 9748250]
28. Cantrell AR, Tibbs VC, Westenbroek RE, Scheuer T, Catterall WA. Dopaminergic modulation of voltage-gated Na+ current in rat hippocampal neurons requires anchoring of cAMP-dependent protein kinase. J Neurosci. 1999; 19:RC21. [PubMed: 10460275]
29. Henn V, et al. Identification of a novel A-kinase anchoring protein 18 isoform and evidence for its role in the vasopressin-induced aquaporin-2 shuttle in renal principal cells. J Biol Chem. 2004; 279:26654–26665. [PubMed: 15037626]
30. Lygren B, et al. AKAP complex regulates Ca(2+) re-uptake into heart sarcoplasmic reticulum. EMBO Rep. 2007
31. Stefan E, et al. Compartmentalization of cAMP-dependent signaling by phosphodiesterase-4D is involved in the regulation of vasopressin-mediated water reabsorption in renal principal cells. J Am Soc Nephrol. 2007; 18:199–212. [PubMed: 17135396]
32. Cuff JA, Clamp ME, Siddiqui AS, Finlay M, Barton GJ. JPred: a consensus secondary structure prediction server. Bioinformatics. 1998; 14:892–893. [PubMed: 9927721]
33. Kelley LA, MacCallum RM, Sternberg MJ. Enhanced genome annotation using structural profiles in the program 3D-PSSM. J Mol Biol. 2000; 299:499–520. [PubMed: 10860755]
34. Koonin EV, Gorbalenya AE. Related domains in yeast tRNA ligase, bacteriophage T4 polynucleotide kinase and RNA ligase, and mammalian myelin 2',3'-cyclic nucleotide phosphohydrolase revealed by amino acid sequence comparison. FEBS Lett. 1990; 268:231–234. [PubMed: 2166684]

35. Holm L, Sander C. Protein structure comparison by alignment of distance matrices. J Mol Biol. 1993; 233:123–138. [PubMed: 8377180]
36. Rehse PH, Tahirov TH. Structure of a putative 2'–5' RNA ligase from Pyrococcus horikoshii. Acta Crystallogr D Biol Crystallogr. 2005; 61:1207–1212. [PubMed: 16131753]
37. Kato M, et al. Crystal structure of the 2'–5' RNA ligase from Thermus thermophilus HB8. J Mol Biol. 2003; 329:903–911. [PubMed: 12798681]
38. Hofmann A, et al. Structure and mechanism of activity of the cyclic phosphodiesterase of Appr>p, a product of the tRNA splicing reaction. Embo J. 2000; 19:6207–6217. [PubMed: 11080166]
39. Kozlov G, et al. Solution structure of the catalytic domain of RICH protein from goldfish. Febs J. 2007; 274:1600–1609. [PubMed: 17480208]
40. Sakamoto Y, Tanaka N, Ichimiya T, Kurihara T, Nakamura KT. Crystal structure of the catalytic fragment of human brain 2',3'-cyclic-nucleotide 3'-phosphodiesterase. J Mol Biol. 2005; 346:789–800. [PubMed: 15713463]
41. Mazumder R, Iyer LM, Vasudevan S, Aravind L. Detection of novel members, structure-function analysis and evolutionary classification of the 2H phosphoesterase superfamily. Nucleic Acids Res. 2002; 30:5229–5243. [PubMed: 12466548]
42. Jung DJ, et al. Novel transcription coactivator complex containing activating signal cointegrator 1. Mol Cell Biol. 2002; 22:5203–5211. [PubMed: 12077347]
43. Hofmann A, Grella M, Botos I, Filipowicz W, Wlodawer A. Crystal structures of the semireduced and inhibitor-bound forms of cyclic nucleotide phosphodiesterase from Arabidopsis thaliana. J Biol Chem. 2002; 277:1419–1425. [PubMed: 11694509]
44. Hardie DG, Hawley SA, Scott JW. AMP-activated protein kinase--development of the energy sensor concept. J Physiol. 2006; 574:7–15. [PubMed: 16644800]
45. Barford D, Johnson LN. The allosteric transition of glycogen phosphorylase. Nature. 1989; 340:609–616. [PubMed: 2770867]
46. Frederich M, Balschi JA. The relationship between AMP-activated protein kinase activity and AMP concentration in the isolated perfused rat heart. J Biol Chem. 2002; 277:1928–1932. [PubMed: 11707445]
47. Sergienko EA, Srivastava DK. Kinetic mechanism of the glycogen-phosphorylase-catalysed reaction in the direction of glycogen synthesis: co-operative interactions of AMP and glucose 1-phosphate during catalysis. Biochem J. 1997; 328(Pt 1):83–91. [PubMed: 9359837]
48. DeFranco DB. Navigating steroid hormone receptors through the nuclear compartment. Mol Endocrinol. 2002; 16:1449–1455. [PubMed: 12089341]
49. Lange A, et al. Classical nuclear localization signals: definition, function, and interaction with importin alpha. J Biol Chem. 2007; 282:5101–5105. [PubMed: 17170104]
50. The CCP4 suite: programs for protein crystallography. Acta Crystallogr D Biol Crystallogr. 1994; 50:760–763. [PubMed: 15299374]
51. Emsley P, Cowtan K. Coot: model-building tools for molecular graphics. Acta Crystallogr D Biol Crystallogr. 2004; 60:2126–2132. [PubMed: 15572765]

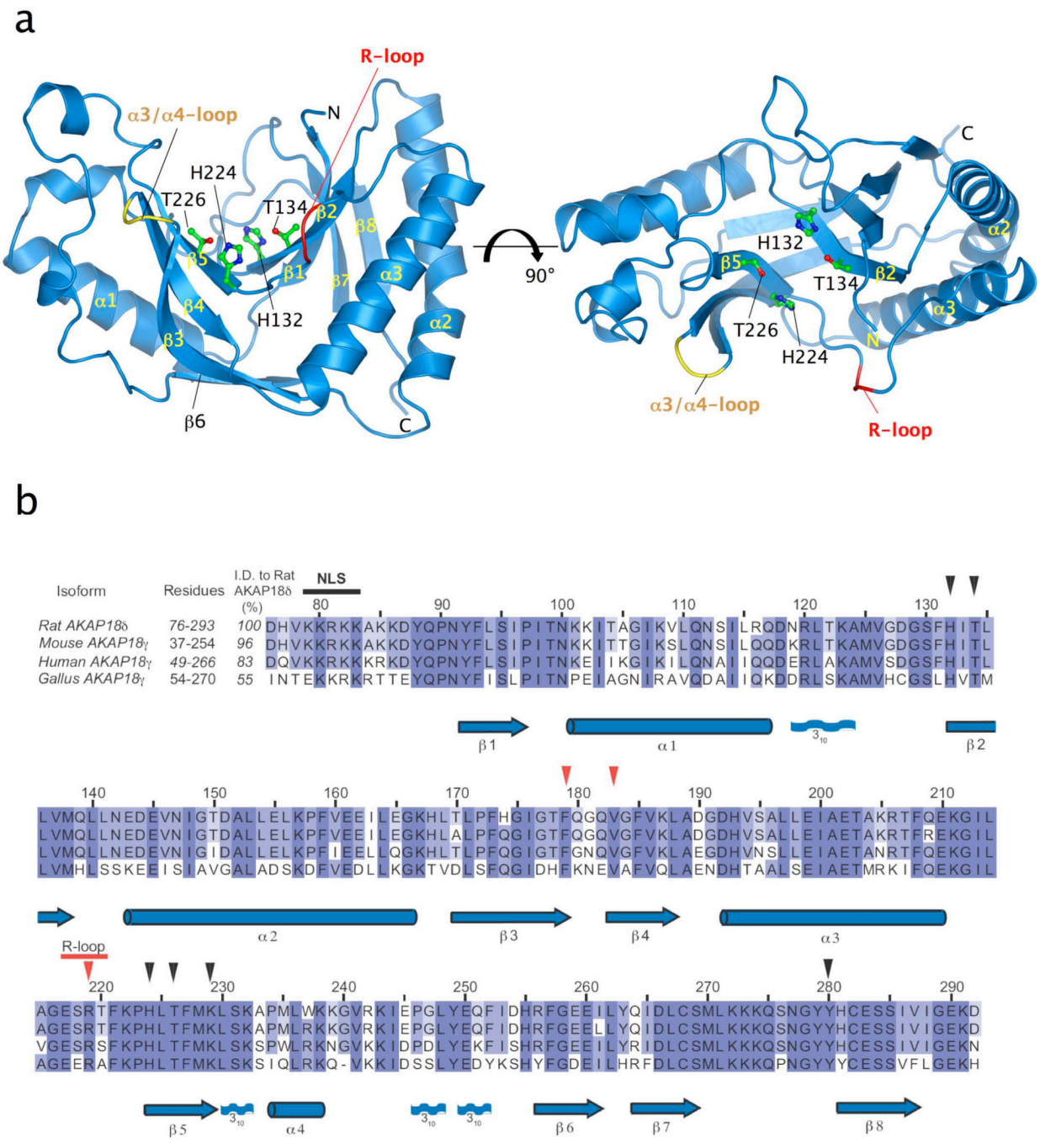

Figure 1. Structural overview

(A) Ribbons representation of the AKAP18δ central domain. The His-x-Thr motifs, N and C-termini, secondary structure elements and R- and α3/α4 loops are labelled. (B) Multiple sequence alignment of mammalian AKAP18 homologues of various species. Residues are coloured by percentage identity. The positions of the R-loop and NLS are indicated. Triangles denote the positions of conserved residues lining the binding groove that either directly contact or form water-mediated hydrogen bonds to the phosphate (black) and adenosine (red) moieties of 5'AMP in the complex crystal structure.

a

Nucleotide	Concentration	Electron density
5' AMP	5 mM	Yes
5' CMP	5 mM	Yes
5' GMP	5 mM	No
5' TMP	5 mM	No
3'–5' cAMP	5 mM	No
Rp-cAMPS	5 mM	No
ATP	5 mM	No
ADP	5 mM	No
2'–3' cCMP	5 mM	No
2'–3' cNADP	5 mM	No
2'–3' cCMP & 3' AMP	Both 5 mM	No
3' AMP	5 mM	No
5' AMP	670 μM	Yes
5' AMP	40 μM	No
5' AMP	10 μM	No

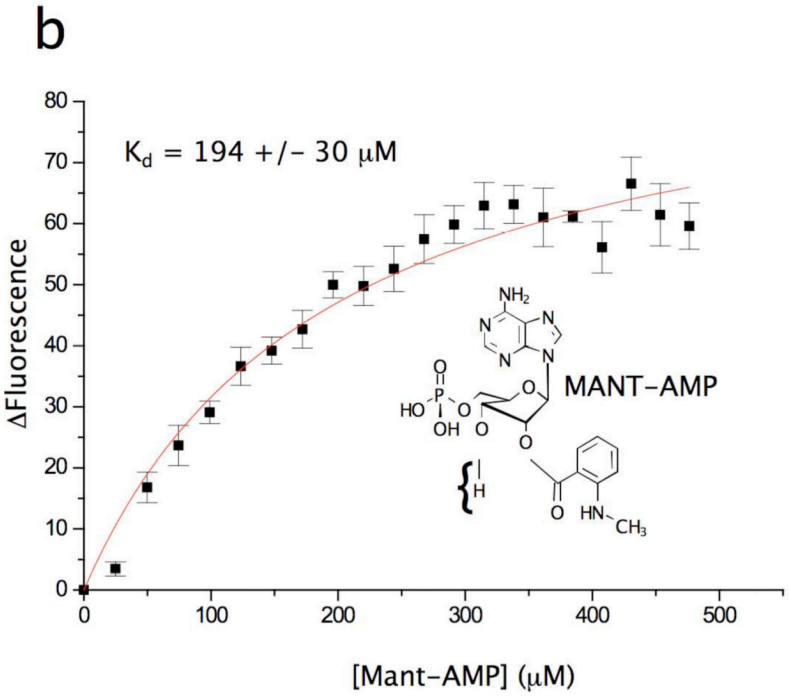

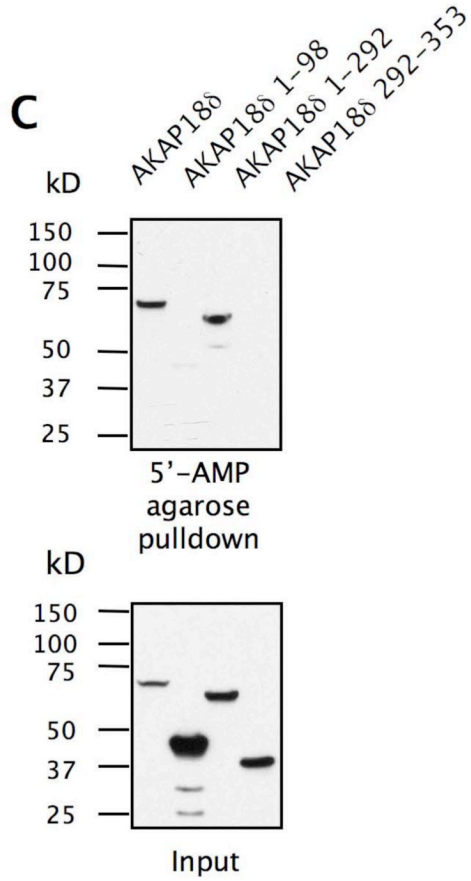

Figure 2. Nucleotide Binding properties of the AKAP18δ central domain

(A) Table showing results of co-crystallisation of AKAP18^{CD} with a range of nucleotides at varying concentrations (B) The fluorescence of 25 μM AKAP18^{CD} alone and MANT-AMP alone was subtracted from that of MANT-AMP in the presence of 25 μM AKAP18^{CD} and in this figure, Δfluorescence (arbitrary units), was plotted as a function of total MANT-AMP concentration. The chemical structure of MANT-AMP is shown. (C) Anti-V5 epitope Western blot showing binding of V5 epitope-tagged AKAP18δ constructs to 5'AMP-agarose beads. Isolated regions N(1–98)- and C(292–353)-terminal to the central domain did not bind to the beads.

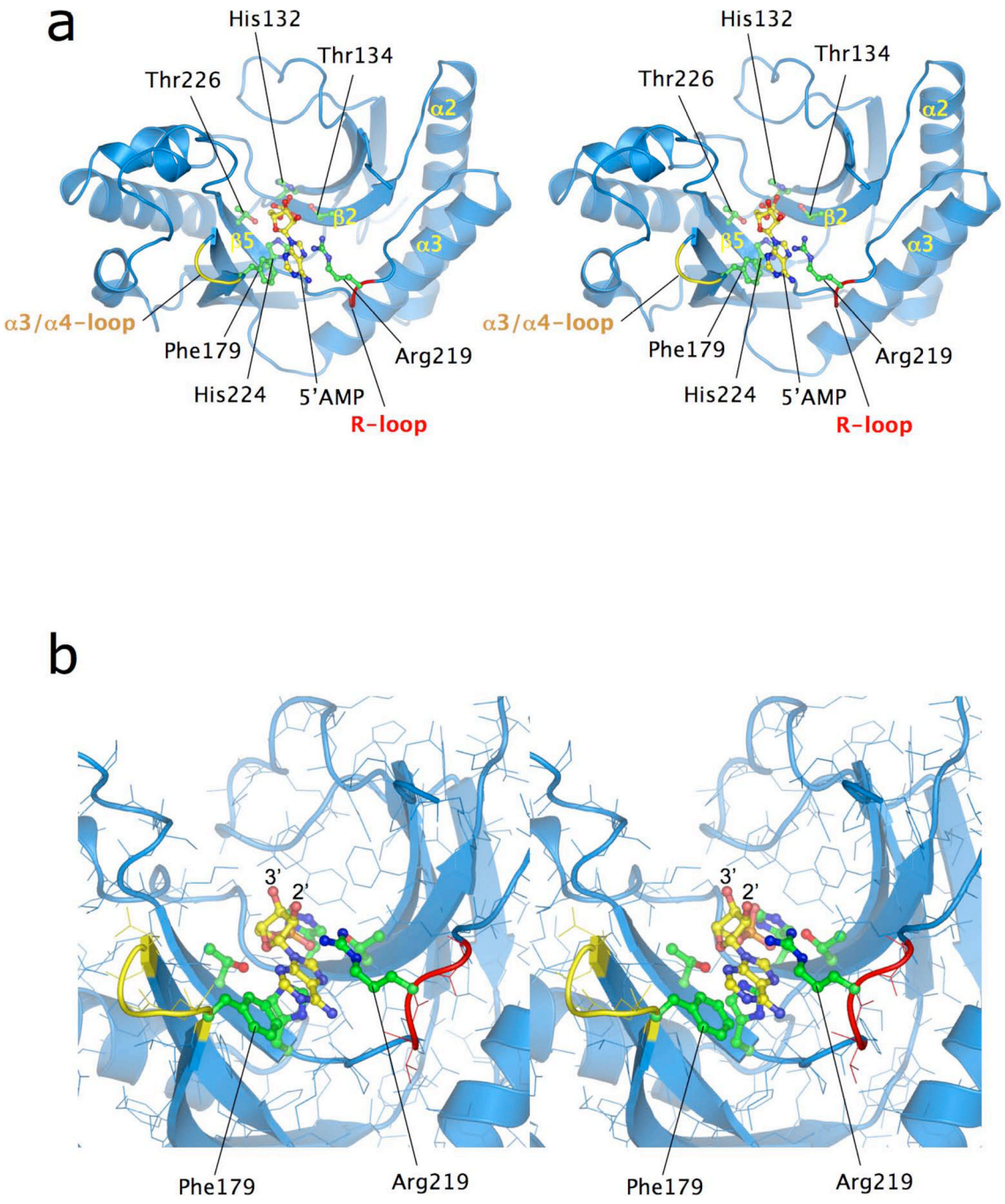

Figure 3. AKAP18δ – AMP complex

(A) Stereoviews of the AKAP18δ central domain in complex with 5'AMP (coloured yellow). The positions of the HxT motifs and Phe179 and Arg219, which sandwich the adenine moiety of 5'AMP, are indicated. (B) Close-up of AMP bound to AKAP18^{CD} with all atoms shown demonstrating accessibility of the O2' and O3' hydroxyls.

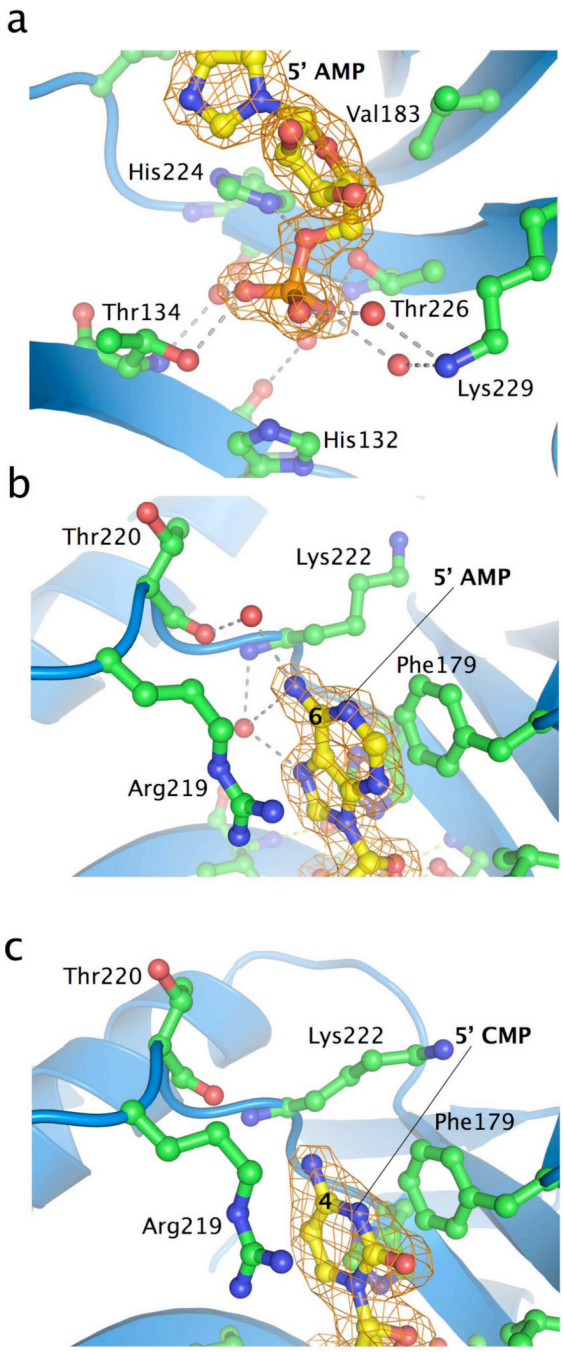

Figure 4. Structural basis for nucleotide binding specificity

Close-ups of the AKAP18δ binding groove in complex with mononucleotides (coloured yellow), centred on the phosphate moiety of 5'AMP (A) and the base moieties of 5'AMP (B) and 5' CMP (C). Hydrogen bonds are indicated by dotted lines, Fo-Fc electron density is contoured at 3σ.

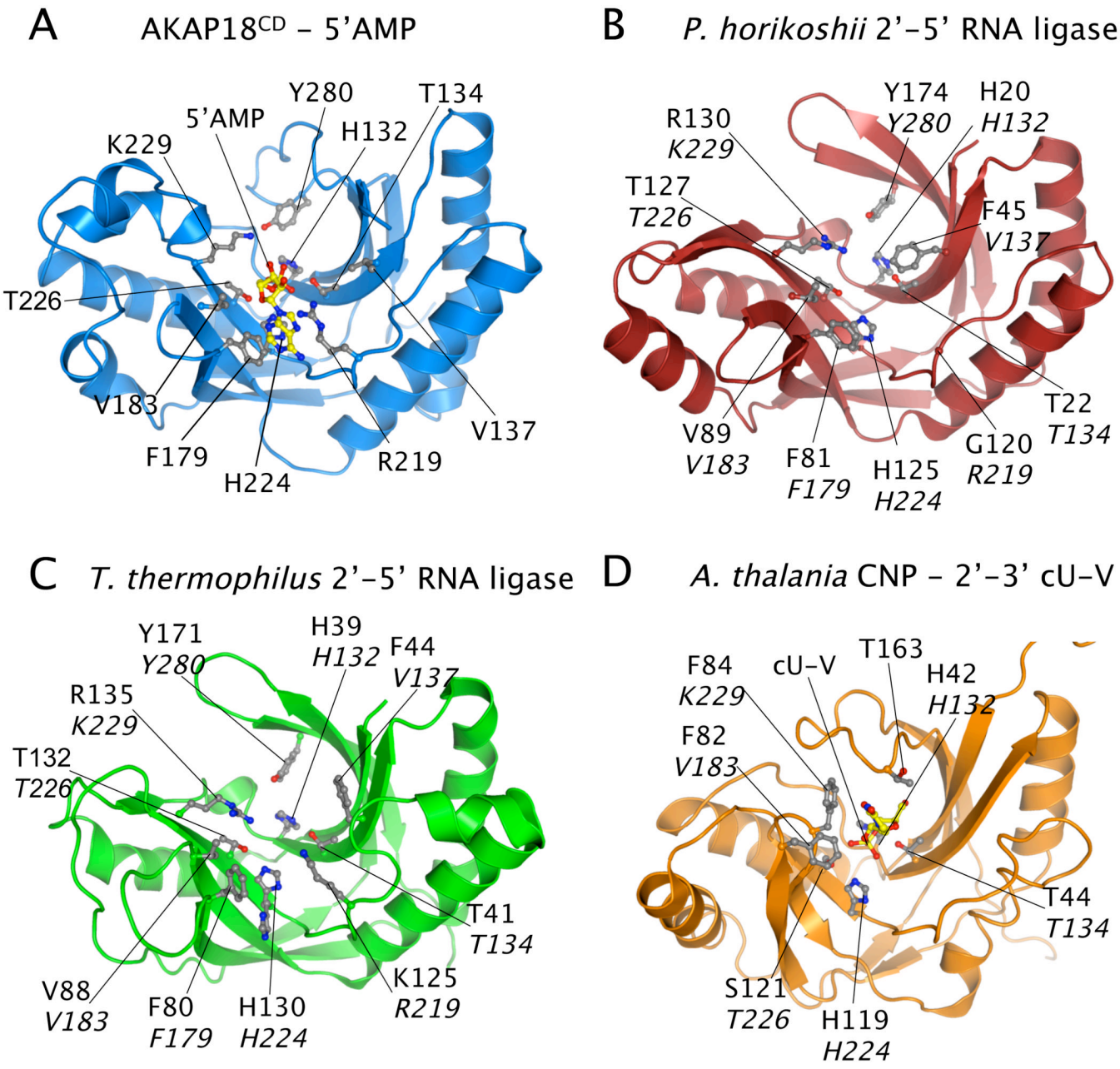

Figure 5. Comparison with 2H phosphoesterase proteins

Equivalent views of the binding groove in four 2H phosphoesterase proteins after superpositions of the conserved His-x-Thr motifs (A) AKAP18δ (blue) in complex with 5'AMP (coloured yellow) (B) *P. horikoshii* 2'–5' RNA ligase (PDB ID 1VDX)[36] (C) T. thermophilus 2'–5' RNA ligase (PDB ID 1IUH)[37] (D) *A. thalania* 1'–2'-cyclic nucleotide 2'-phosphodiesterase in complex with cyclic 2'–3' uridine vanadate (PDB ID 1JH7)[43].

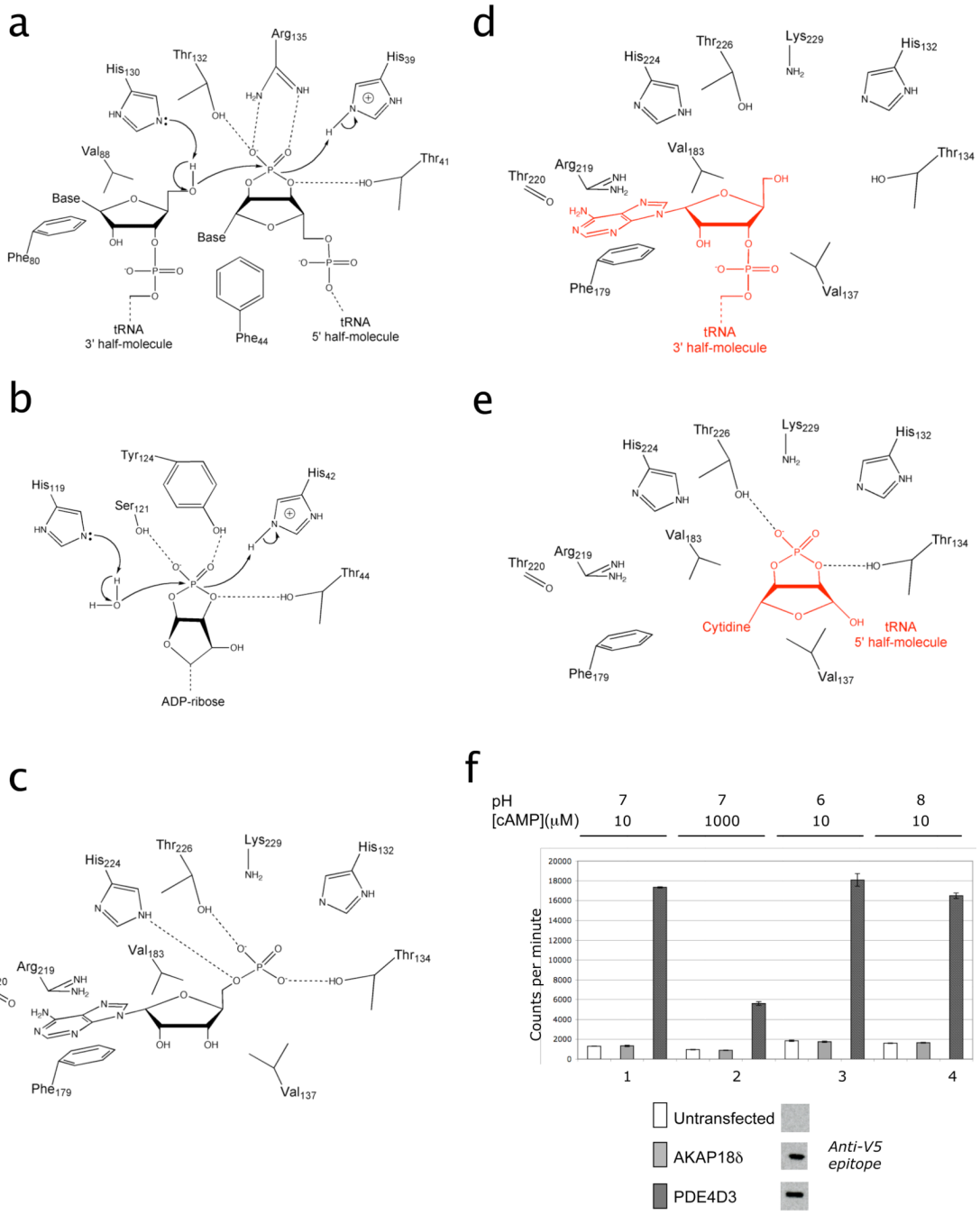

Figure 6. Catalysis by 2H phosphoesterase proteins

Putative catalytic mechanisms for 2'–5' RNA ligase (A) and *Arabidopsis* CNP (B) are illustrated. The position of equivalent residues in the AKAP18δ binding groove, and their role in coordinating 5'AMP, is illustrated (C). Only direct protein-AMP hydrogen-bonds are indicated in the AKAP18^{CD} complex. Binding of 3' AMP and cyclic 2'–3' CMP to AKAP18δ was attempted to test the potential of AKAP18δ to act as a 2'–5' RNA ligase, the rational being that these molecules would mimic 3' (D) and 5' (E) tRNA half-molecules, respectively. (F) AKAP18δ was assayed for cAMP phosphodiesterase activity. Assays were performed using immunoprecipitated V5-epitope tagged full-length AKAP18δ (light grey bars), with different concentrations of cAMP (lanes 1, 2) and at different pH (lanes 1, 3, 4),

in each instance including negative (untransfected, white bars) and positive (PDE4D3, dark grey bars) controls. AKAP18δ activity did not differ significantly from the negative control in any condition.

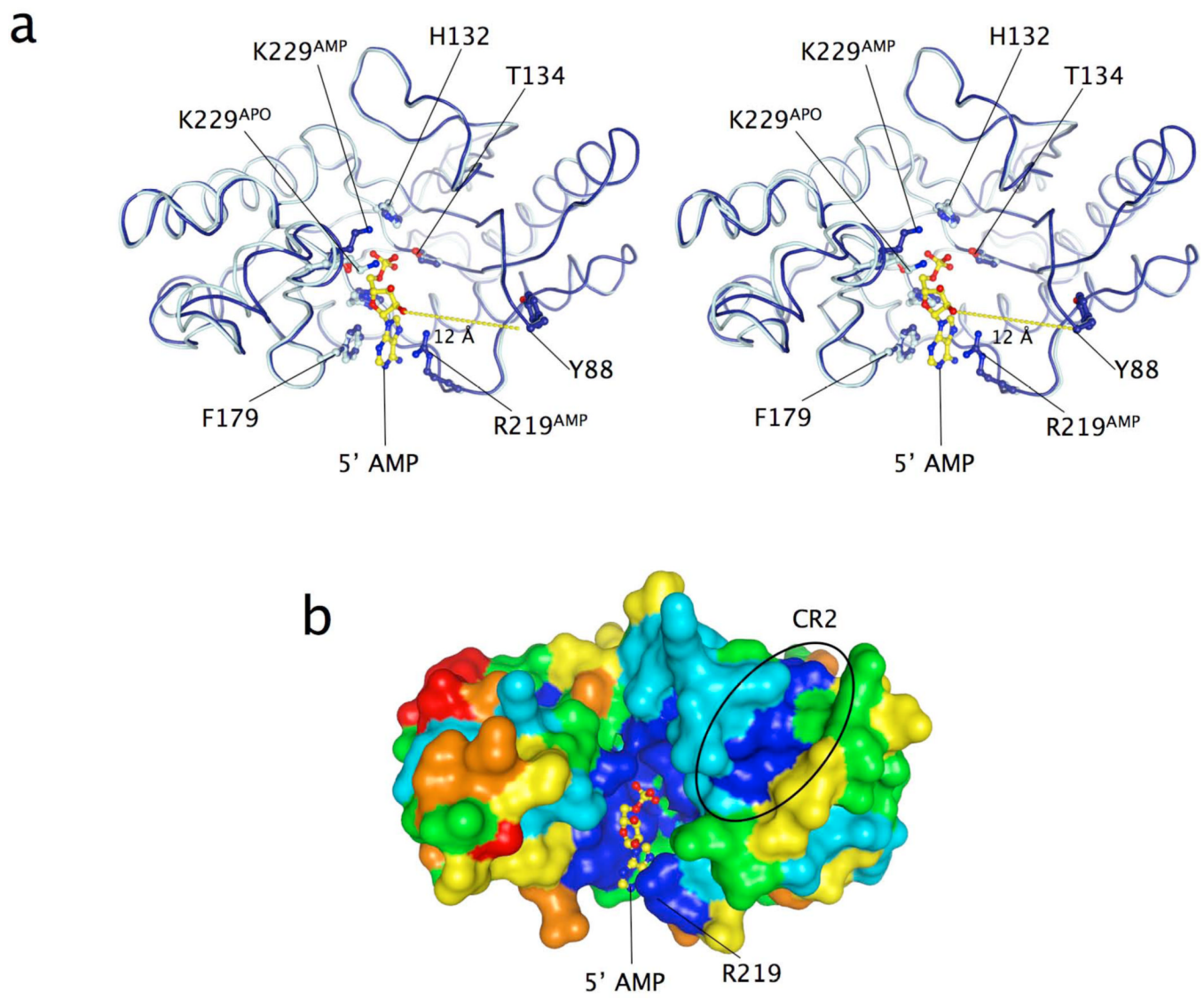

Figure 7. Potential as an 5'AMP sensor

(A) Stereoviews showing structural differences between the AKAP18δ central domain in the apo state (light blue, superscript^{APO}) and in complex with 5'AMP (dark blue, superscript^{AMP}). The distance between C_α of the first residue visible in the electron density at the N-terminus of AKAP18δ (Tyr88) and the ribose 2'-OH group of 5'AMP in the complex structure is indicated, 5'AMP is coloured yellow. (B) Surface representation showing sequence conservation by colour (red is least conserved, blue is most conserved) on AKAP18δ in complex with 5'AMP. The position of Arg219 is indicated to orient the viewer. A highly conserved region adjacent to the nucleotide-binding groove is circled.

Table 1
Bioinformatic analysis of mammalian AKAPs

The longest isoform of each mammalian AKAP was systematically investigated for regions of discrete non-repetitive secondary structure using the secondary structure prediction program JPRED and for regions of potential structural similarity to proteins of known structure by the fold recognition program PHYRE.

AKAP*	Accession Number (total amino acids)	Secondary structure (SS) prediction by JPRED$	Fold recognition by PHYRE# (estimated certainty)
D-AKAP1 (AKAP1)	AAH00729 (903)	Diffuse mixed SS elements throughout	KH domain 605–675 (100%), Tudor domain 760–810 (95%)
AKAP-KL (AKAP2)	NP_001004065 (948)	Dense mixed SS throughout	-
AKAP110 (AKAP3)	NP_006413 (853)	Dense mixed SS throughout	-
AKAP82 (AKAP4)	CAI41561 (854)	Dense mixed SS throughout	-
AKAP150 (AKAP5)	AAB07887 (714)	160–640 no SS	Porin transmembrane β-barrel 255–525 (20%)
mAKAPα (AKAP6)	NP_004265 (2319)	480–615 no SS, 740–1250 helical only, 1250–2319 mixed SS	Spectrin repeats 750–1250 (100%)
AKAP18δ (AKAP7)	AAR06859 (353)	1–70 no SS	Region 90–290 similar to *P. horikoshii* protein similar to 2'–5' RNA ligase (100%), *T. thermophilus* 2'–5' RNA ligase (100%), Appr>r CNP (90%)
AKAP95 (AKAP8)	AAH37270 (692)	360–692 predicted to have dense and predominantly helical SS	-
AKAP450 (AKAP9)	CAB40713 (3908)	Mixed SS up to 150, remaining sequence coiled coil	Aligns with long helical region of colicin1α throughout sequence (100%)
D-AKAP2 (AKAP10)	EAW50913 (662)	Mixed SS throughout	RGS domain 220–360 and 370–510 (both 100%)
AKAP220 (AKAP11)	EAX08676 (1901)	Mixed SS throughout	Sir4 coiled-coil dimerisation motif 480–640 (25%)
Gravin (AKAP12)	NP_005091 (1782)	Mixed SS throughout	Myc box interacting protein 1620–1760 (20%)
AKAP-Lbc (AKAP13)	NP_006729 (2817)	Mixed SS throughout, coiled coil 2350–2400 and 2570–2690	Ankyrin repeat 170–220 (45%), C1 domain 1790–1840 (95%), DH/PH domain 1975–2350 (100%)
AKAP28 (AKAP14)	NP_848928 (197)	Mixed SS throughout	-
BIG2	NP_006411 (1785)	Predominantly helical SS, no SS 210–360	Sec7 domain 635–840 (100%), Armadillo repeats 10–600 (100%)
MAP2	NP_002365 (1827)	Mixed SS throughout with exception of no SS 1480–1600	-
PAP7	AAN60219 (528)	Mixed SS throughout with exception of no SS 10–65	Acyl-CoA-binding domain 85–175 (100%)
Pericentrin B	AAP46636 (3336)	Predominantly coiled-coil throughout	Aligns with long helical region of colicin1α throughout sequence (100%)
RSP3	AAK26432 (418)	Mixed SS throughout	-
WAVE1	NP_001020107 (559)	280–490 no SS	Syntaxin6 25–75 (25%)

*Gene nomenclature committee names are in parentheses.

$Regions of greater than 50 amino acids with no predicted secondary structure are listed.

#Alignments with estimated precision of 10 % or below were discounted - for AKAPs >1200 residues, the sequence was broken into blocks of 1200 amino acids with 400-residue overlaps.

C1, Cysteine-rich phorbol-binding domain; DH, Dbl homology; KH, K homology; PH, Pleckstrin homology; RGS, Regulator of G-protein Signaling.

Table 2
Crystallographic data collection and refinement statistics

Figures for the highest resolution shell are in parentheses.

Data Set	**AKAP18^{CD}**	**Selenium-substituted AKAP18^{CD}**	**AKAP18^{CD} – 5'AMP complex**	**AKAP18^{CD} – 5' CMP complex**
Collection and Phasing Statistics				
X-ray source	ESRF ID14.3	ESRF ID14.2	ESRF ID14.3	ESRF ID14.3
Space group	$P3_1$	$P3_1$	$P3_1$	$P3_1$
Unit cell (Å)	a = b = 42.42, c = 96.91	a = b = 42.61, c = 98.34	a = b = 42.23, c = 97.72	a = b = 42.97, C = 97.97
Z	1	1	1	1
Wavelength (Å)	0.9794	0.9330	0.9794	0.9794
Resolution (Å)	1.80	2.10	1.50	2.25
Observations (N)	49322 (7318)	136308 (16456)	84120 (12321)	38757 (5420)
Unique Reflections (N)	18073 (2654)	11263 (1426)	31159 (4543)	9559 (1391)
Completeness (%)	99.7 (99.9)	96.9 (85.4)	99.7 (100.0)	99.5 (98.4)
R_{merge}	0.043 (0.272)	0.052 (0.281)	0.039 (0.323)	0.091 (0.297)
I/σ(I)	17.7 (3.1)	38.5 (9.1)	18.2 (2.5)	13.6 (5.2)
Anomalous Completeness (%)	-	96.0 (83.4)	-	-
Anomalous multiplicity	-	5.7 (5.3)	-	-
DelAnom correlation between half-sets	-	0.805 (0.520)	-	-
Selenium sites (N)	-	5	-	-
Refinement Statistics				
Resolution Range (Å)	97.13 – 1.80		97.59 – 1.50	98.06 – 2.25
Reflections (N)	17152		29583	9095
Number of non-hydrogen atoms	1710		1863	1689
Working R value	0.206		0.161	0.225
Free R value (N reflections)	0.238 (921)		0.209 (1570)	0.261 (460)
Deviation from ideality Bond lengths (Å) Bond angles (°)	 0.010 1.252		 0.015 1.590	 0.015 1.721
B factor averages (Å^2)	31.3 (total) 36.6 (waters)		20.2 (total) 30.5 (waters) 18.5 (5'AMP)	19.3 (total) 17.9 (waters) 32.3 (5'CMP)
Ramachandran values (%) [preferred/ allowed/generously allowed/disallowed]	91.6/8.4/0/0		92.2/7.8/0/0	93.9/6.1/0/0